Journal of Materials Chemistry A

COMMUNICATION

View Article Online
View Journal | View Issue

Cite this: J. Mater. Chem. A, 2018, 6, 19934

Received 16th August 2018
Accepted 28th September 2018

DOI: 10.1039/c8ta07954d

rsc.li/materials-a

Ultra-narrow bandgap non-fullerene organic solar cells with low voltage losses and a large photocurrent†

Jianqiu Wang,‡[ab] Shenkun Xie,‡[ab] Dongyang Zhang,[ab] Rong Wang,[ab] Zhong Zheng,[b] Huiqiong Zhou[b] and Yuan Zhang*[a]

Organic solar cells (OSCs) with ultra-narrow band gaps (UN-BGs) often suffer from higher energy losses and resulting inferior power conversion efficiencies (PCEs) compared to mid-bandgap systems. Benefiting from an optimal balance between the photocurrent and energy losses, OSCs based on the bulk heterojunction PTB7-Th : IEICO-4F with an effective bandgap of 1.03 eV can produce an impressive PCE of greater than 11%, which is on a par with that found in mid-gap non-fullerene devices with an 3,9-bis(4-(1,1-dicyanomethylene)-3-methylene-2-oxo-cyclopenta[*b*]thiophen)-5,5,11,11-tetrakis(4-hexylphenyl)-dithieno[2,3-*d*′:2,3-*d*′]-*s*-indaceno[1,2-*b*:5,6-*b*′]-dithiophene (ITCC) acceptor. The supreme solar harvesting observed in the IEICO-4F device can be correlated to a reduced bi-molecular recombination rate constant alongside low voltage losses (<0.4 V). On the other hand, the poor fill factor observed when using an IEICO-4F acceptor seems to be connected to a stronger field-dependence on the charge extraction and an enlarged energetic disorder. To this end, further improvements in the PCE of OSCs using UN-BG acceptors could be prompted by improving the charge sweepout, which could be enabled by increasing the charge transport properties with optimized nanomorphology.

Organic bulk heterojunction (BHJ) organic solar cells (OSCs) with non-fullerene acceptors (NFA) possess a particular ability to capture larger numbers of photons due to the improved absorption overlap with respect to the solar spectrum. Owing to the intrinsic trade-off between the short-circuit current (J_{sc}) and the open-circuit voltage (V_{oc}),[1] the effective band gap, or E_g(eff) (which from here is defined as the energy offset between the highest occupied molecular orbital (HOMO) in the donor and the lowest unoccupied molecular orbital (LUMO) in the acceptor) is ranged between 1.5–1.6 eV in representative high efficiency OSCs that have power conversion efficiencies (PCEs) greater than 12%.[2–13] In comparison to these mid-bandgap bulk heterojunctions (BHJs), OSCs based on acceptors with an ultra-narrow bandgap (UN-BG) generally suffer from higher energy losses,[14,15] resulting in poor PCEs.[16–20] Very recently, an interesting UN-BG acceptor adopting the A–D–A structure (abbreviated as IEICO-4F) has been demonstrated, which upon blending with the narrow bandgap PTB7-Th donor can produce PCEs of over 10%.[21] The fluorination of IEICO-4F leads to the HOMO and LUMO energies being pushed down to 5.45 eV and 4.2 eV, respectively, effectively reducing the E_g(eff) but leaving a sufficient HOMO–HOMO offset to allow a hole transfer.[21,22] Coupling this molecular strategy to a interfacial modification with doping, we recently showed that the power conversion efficiency (PCE) in PTB7-Th : IEICO-4F solar cells can be further boosted to more than 12% with an impressive J_{sc} exceeding 26 mA cm^{-2}.[23]

From a fundamental standpoint, while the reduction in E_g(eff) helps to extend the absorption onset to the lower energy regime with potential gains in the absorbed photon density, it is a prerequisite that the generated excitons should be effectively dissociated into mobile carriers, and eventually extracted *via* the electrodes to render a photocurrent. In OSCs, the fate of carriers is subject to the competing results of the charge extraction and recombination. The general relationship of the recombination rate B is described by the following equation, $B = \beta np$, in which β is the recombination rate constant and np are the densities of the electron and hole, respectively.[24] For UN-BG devices, the enlarged densities of excitons and resultant photo-carriers could be a concern, namely because np may give rise to an elevation of the bi-molecular recombination. In fullerene based OSCs, understanding the non-geminate bi-molecular recombination has enabled researchers to obtain insights into the losses of photo-carriers and eventual PCEs, as well as the factors limiting the fill factor (FF).[25] Owing to the high photo-current in IEICO-4F based OSCs, the ultimate PCE tends to be

[a]School of Chemistry, Beijing Advanced Innovation Center for Biomedical Engineering, Beihang University, Beijing 100191, P. R. China. E-mail: yuanzhang@buaa.edu.cn
[b]CAS Key Laboratory of Nanosystem and Hierachical Fabrication, CAS Center for Excellence in Nanoscience, National Center for Nanoscience and Technology, Beijing 100190, P. R. China

† Electronic supplementary information (ESI) available: Experimental methods, supporting figures and notes. See DOI: 10.1039/c8ta07954d

‡ The authors contributed equally to this work.

mainly limited to the two parameters of V_{oc} and FF. In previous studies, both the V_{oc} and FF have been correlated to the recombination dynamics in OSCs with PCBM acceptors.[26] In this context, it will be of interest to probe non-geminate recombination and the impact on the photovoltaic performance in non-fullerene UN-BG systems. Owing to a range of NFAs with different LUMO energies, a systematic variation on E_g(opt) is enabled, which prompted us to investigate the correlations between non-geminate (bi-molecular) recombination, carrier transport and extraction, and ultimately photovoltaic performance recombination.

As a testbed for this study, we chose UN-BG solar cells based on PTB7-Th : IEICO-4F blends and two mid-gap BHJs comprising of PBDB-T : ITCC and PTB7-Th : $PC_{71}BM$ blends.[27,28] The chemical structure and energy diagram for the utilized compounds are provided in Fig. 1 and 2a, respectively, using HOMO and LUMO values taken from the literature.[21,22,27] Based on these energetic values, the E_g(eff) values were roughly estimated to be 1.03, 1.57, and 1.12 eV for PTB7-Th : IEICO-4F, PBDB-T : ITCC, and PTB7-Th : $PC_{71}BM$, respectively. As will be seen, the variation of E_g(eff) by more than half an eV enables the extension of the absorption onset to almost an infrared regime (~1000 nm) for PTB7-Th : IEICO-4F. This allows the photo-carrier density to increase by almost one order of magnitude when compared to the other solar cells. Fig. 2b displays the normalized thin film absorption of the three blend films, the absorption of the neat donor and acceptor films are provided in Fig. S1 in the ESI.† It should be noted that the absorption of PTB7-Th : IEICO-4F allows a large portion of the solar spectrum to be captured, which is beneficial for J_{sc}.[23] It is also noteworthy that for the ITCC acceptor, we chose PBTB-T as the donor instead of PTB7-Th. This is because PTB7-Th : ITCC tends to be associated with more severe geminate recombination losses, this is probably due to the low LUMO–LUMO offset or morphological reasons, which complicate our recombination analysis.

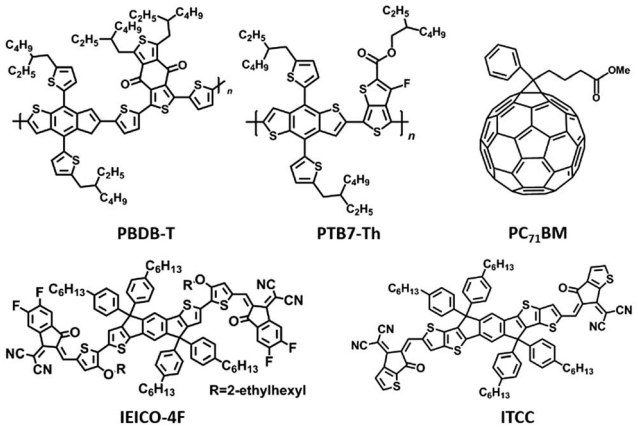

Fig. 1 Chemical structures of the compounds utilized in this study.

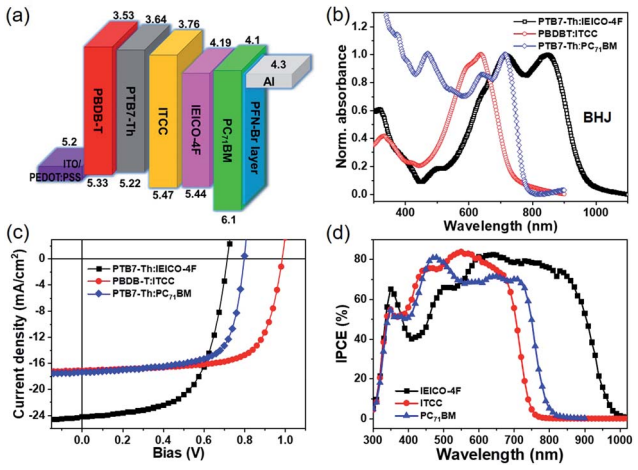

Fig. 2 (a) Energy diagram of solar cells using values of HOMO and LUMO energies taken from the literature. (b) Thin film absorption spectra of various blend films. (c) Current density *versus* voltage (*J*–*V*) characteristics of solar cells measured at a standard 1.5 AM G solar irradiation. (d) Incident photon-to-current efficiency (IPCE) of the respective devices.

Next, we examined the photovoltaic performance of these BHJ films with different E_g(eff). The donor/acceptor (D/A) ratios were optimized at 1 : 1.5, 1 : 1, and 1 : 1.5 for the IEICO, ITCC and $PC_{71}BM$ devices, respectively. More details of the device optimization can be found in the ESI.† Fig. 2c shows the solar cell *J*–*V* characteristics measured at standard AM 1.5G solar illumination (100 mW cm^{-2}). The extracted photovoltaic parameters are summarized in Table 1. As shown, the V_{oc} decreases with reduced E_g(eff) and the largest V_{oc} was found for the PBDB-T : ITCC device, owing to the shallower electron affinity in the ITCC. As expected, we observed a reverse dependence for the J_{sc} on the E_g(eff), with the PTB7-Th : IEICO-4F cell producing the highest J_{sc} of 25.5 mA cm^{-2}, this result was in agreement with the previously reported results.[23] These observations are in line with the general tendencies found for OSCs.[11,13,19] As for the FF, all of the concerned devices exhibited fill factors exceeding 60%. In addition, an interesting tendency was noted that the FF appears to be inversely proportional to the E_g(eff), that is, a higher FF of 71.3% is found for an ITCC with a larger E_g(eff). We attained comparable PCEs in the PTB7-Th : IEICO-4F (11.13%) and PBDB-T : ITCC (11.285%) devices, which primarily result from the increased J_{sc} when using IEICO-4F and V_{oc} with a mid-gap ITCC. Fig. 2d displays the incident photon-to-current efficiency (IPCE) spectra of the solar cells. The maximal IPCE for the two non-fullerene cells both exceed 80%, in particularly for the IEICO-4F cells showing high values of between 75–80% in a wide spectral range (600–850 nm). This can be indicative of efficient photon-harvesting.

Table 1 Solar cell parameters extracted from *J*–*V* curves in Fig. 1d alongside the *E*g(eff) of various BHJ blends

BHJ	V_{oc} (V)	J_{sc} (mA cm^{-2})	FF (%)	PCE (%)	E_g(eff) (eV)
PTB7-Th : IEICO-4F	0.72	25.16	61.45	11.13	1.03
PBDB-T : ITCC	0.98	16.14	71.32	11.28	1.57
PTB7-Th : $PC_{71}BM$	0.80	17.44	69.03	9.63	1.12

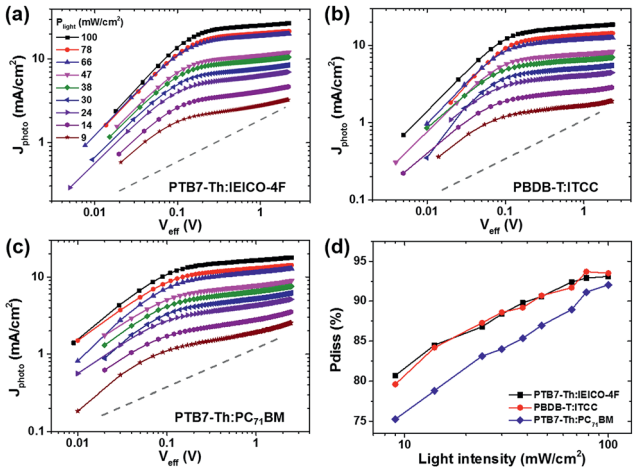

Fig. 3 (a)–(c) Photocurrent (J_{photo}) *versus* effective bias (V_{eff}) characteristics of solar cells based on active layers of PTB7-Th : IEICO-4F (a), PBDB-T : ITCC (b), and PBDB-T : $PC_{71}BM$ (c) (see definitions for J_{photo} and V_{eff} in the main text). Dashed lines were guided by the eye with a slope = 0.5 to illustrate the formation of a space-charge limited photocurrent. (d) Charge dissociation probability (P_{diss}) of solar cells at different light intensities.

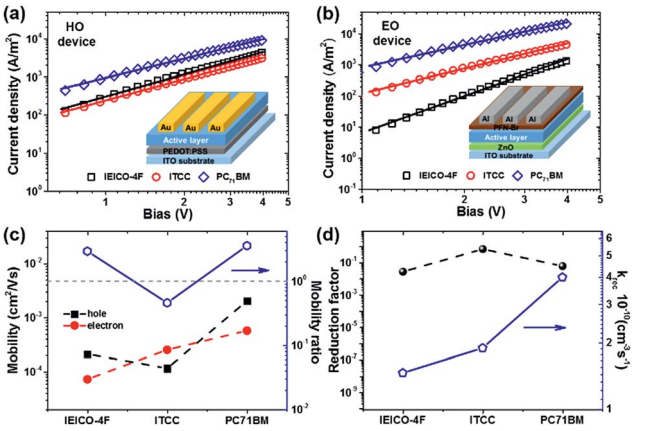

Fig. 4 Dark J–V characteristics of (a) hole-only device (HO) and (b) electron-only (EO) device with similar thicknesses of active layer alongside the SCLC fitting. The insets shown in (a) and (b) are illustrated device structures of the HO and EO, respectively. (c) Steady-state carrier mobility in various blend films along with the mobility ratio of holes to electrons. For ease of comparison, a horizontal dashed line denoting an equal mobility for the two carriers is included. (d) Reduction factor with respect to the Langevin rate and the actual bimolecular recombination rate constant (k_{rec}) in different solar cells.

To better understand the results of the IPCE, in Fig. 3a–c the illumination dependent photocurrent (defined as $J_{photo} = J_{light} - J_{dark}$) against the effective bias V_{eff} (defined here as being $V_{eff} = V_0 - V_{app}$, in which V_0 is the voltage corresponding to $J_{photo} = 0$, as described for the flat band condition) was plotted. At different light intensities, we could not observe any visible square root dependence on J_{photo}, which helped to rule out the space-charge effect. Based on the J_{photo} *versus* V_{eff} characteristics, the charge dissociation probability (P_{diss}) can be extracted by normalizing J_{photo} with respect to J_{sat}, according to the relationship of $P_{diss} = J_{photo}/J_{sat}$, in which J_{sat} is the saturated photocurrent at a large reverse bias.[2] In Fig. 3d, we plotted the determined P_{diss} at a short-circuit condition. Near 1 sun, the P_{diss} in all of the three devices is more than 90%, which to some degree can be correlated to the high external quantum efficiency (EQE). At lower light intensities, the P_{diss} becomes smaller, probably suggesting a carrier density dependent charge dissociation process. Another likely explanation for the reduced P_{diss} at low irradiation may be due to the charge-density dependent mobility in the concerned BHJ films that tends to change the recombination at different carrier densities.[29,30] We observed similar P_{diss} in the two non-fullerene cells, both of which were superior to the $PC_{71}BM$ device. This more efficient charge dissociation may enable potential application of non-fullerene OSCs at low irradiation conditions (see plots of PCE and solar parameters against light intensity in Fig. S2d, ESI†).

As charge recombination strongly depends on the transport properties in the BHJ, we examined the steady-state carrier mobility in these solar cells. Fig. 4a and b display the dark J–V characteristics of the hole-only (see device sketch in the inset of Fig. 4a) and the electron-only (see inset in Fig. 4b) devices based on the same set of BHJ films used for the solar cells. The hole and electron mobilities (denoted as μ_h and μ_e respectively) were extracted based on the Mott–Gurney law in the space charge limited current (SCLC) regime and the results are shown in Fig. 4c. It is surprising to note that PTB7-Th : $PC_{71}BM$ possesses the largest mobilities among the three blends, with the μ_h being 2.03×10^{-3} cm^2 V^{-1} s^{-1} and the μ_e being 5.7×10^{-4} cm^2 V^{-1} s^{-1}. We observed slightly reduced mobilities in the order of 10^{-4} cm^2 in the two non-fullerene BHJs. Given the small thickness of the active layer around 100 nm, the mobility in the range of 10^{-3}–10^{-4} cm^2 V^{-1} s^{-1} could be sufficient for a charge sweepout. As seen from Fig. 4c, which shows the ratios of the hole mobility to that of the electrons, the differences between μ_h to μ_e are less than an order. The balanced transport in these BHJs could minimize the space-charge effects in solar cells under illumination, which is in agreement with the results shown in Fig. 3c–e. In our previous investigations, we showed that an increase in the mobility imbalance in OSCs tends to be associated with a stronger reduction factor, γ, with respect to the Langevin recombination rate, eventually leading to a smaller recombination rate constant.[31] In the BHJs, the deviation from classical Langevin theory could be related to the imbalanced transport and phase separation and such a phenomenon can be described by the dimensionless parameter y, defined by the ratio of k_{rec} to k_L.[32] Using this knowledge, we determined the value of γ based on an analytical model proposed by Blom *et al.*,[33] (see detailed method and mobility of double carrier devices (solar cells) in Fig. S3 and ESI†). Fig. 4d shows the extracted γ in the BHJ blends and the extracted recombination rate constants in all cases obviously deviate from the calculated Langevin rate, with the γ falling in the 10^{-2}–10^{-1} range. We observed the strongest reduction (with the lowest γ of 0.027) in the IEICO-4F based device, followed by a value of $\gamma = 0.06$ in the $PC_{71}BM$ device, and the largest γ of 0.68 was found in the ITIC cell. The weakest reduction in the ITCC device seems to be correlated to the smaller μ_h (with respect to μ_e), whereas the other two BHJs possess a larger μ_h. Irrespective of the

microscopic origins, a smaller γ benefits the reduction of the bimolecular recombination rate constant. We further determined the actual rate constant according to $k_{rec} = \gamma k_L$, in which k_L is the Langevin rate constant described by the following equation:[31,32]

$$k_L = \frac{q}{\varepsilon_o \varepsilon_s}(\mu_h + \mu_e) \quad (1)$$

For all of the compared solar cells, the extracted k_{rec} falls in the order of 10^{-10} cm^{-3} s^{-1} with the smallest k_{rec} of 1.46×10^{-10} cm^{-3} s^{-1} being found in the IEICO-4F cell, followed by that of the ITCC (1.9×10^{-10} cm^{-3} s^{-1}). The k_{rec} of $PC_{71}BM$ solar cell showed the highest value of 3.99×10^{-10} cm^{-3} s^{-1}. It should be noted that the k_{rec} seems to be in accordance with the J_{sc} and IPCE. This correlation may suggest the importance of the reduced k_{rec} for mitigating carrier losses *via* bi-molecular recombination.

Having obtained insights into the photo-carrier losses through steady-state transport analysis, next we explored the recombination kinetics to understand the impact on the FF. In fullerene based OSCs, the FF has been correlated to the interplaying processes of charge transport, recombination and extraction which all occur in a BHJ film with a phase-segregated and inter-percolated nanomorphology.[16] As the FF basically describes how the photocurrent evolves with varied voltages, it is informative to probe the process of a carrier sweepout at various biases. Fig. 4a comparatively shows the normalized transient photocurrents (TPCs). If the recombination is unchanged, one would expect an overlap in these decay traces. Notable differences were observed at early decay times or decay tails, as shown in the inset of Fig. 5a, which can indicate distinct recombination kinetics in these solar cells. By performing the transient photocurrent (TPC) measurements at various biases (see results in Fig. S4, ESI†), we obtained information related to the dependence of the electrical field on the charge sweepout process. The decay time reflected in the TPC measurements contains both contributions from the charge extraction and recombination. While in the short-circuit condition, the latter tends to be less significant. Based on a mono-exponential decay model, the extracted lifetime for TPC (τ_{tpc}) was plotted against the applied bias in Fig. 5b. In all devices, the τ_{tpc} becomes longer with an increase in the forward bias and in contrast a weaker field-dependent τ_{tpc} is noted under the reverse bias. This trend could be mainly due to a suppressed recombination at higher internal fields. Among these solar cells, the ITCC device exhibits a faster extraction at all biases. The slower τ_{tpc} in the $PC_{71}BM$ cell may be correlated to the larger bimolecular recombination rate constant. For the UN-BG cells with IEICO-4F, we observed the notable feature that the τ_{tpc} displays a more significant field-dependence in the forward bias regime with a τ_{tpc} exceeding 100 ns near the flat-band condition. This result seems to suggest that charge extraction is impeded at reduced electrical fields in the UN-BG device. As a result, those (non-extracted) carriers tend to accumulate inside the active layer, raising the recombination close to the V_{oc}. It should be mentioned that the slower charge extraction in the IEICO-4F device only occurs at lower electrical fields, that is near V_{oc}, while in the near short-circuit condition the charge sweepout is still efficient, given the considerably reduced τ_{tpc}, which is consistent with the high J_{sc} with a lower recombination rate constant. Based on the results of the TPC, the dependence of the τ_{tpc} on the bias can be correlated to the FF in the solar cells and the impeded sweepout at low electrical fields is seemingly one of the limiting factors for the FF in UN-BG solar cells with IEICO-4F. Currently, there is not a full explanation for the more efficient charge sweepout in the ITCC device. It could be related to an optimal balance between the charge recombination and transport or a higher crystallinity in the ITIC acceptor. In our TPC measurements, a pulsed laser (488 nm) was used for photo-excitation and the resulting exciton density may differ from the situation in operational solar cells under solar irradiation. Further studies using TPC with continuous white light bias may be needed to elaborate the exact mechanism for these observations.

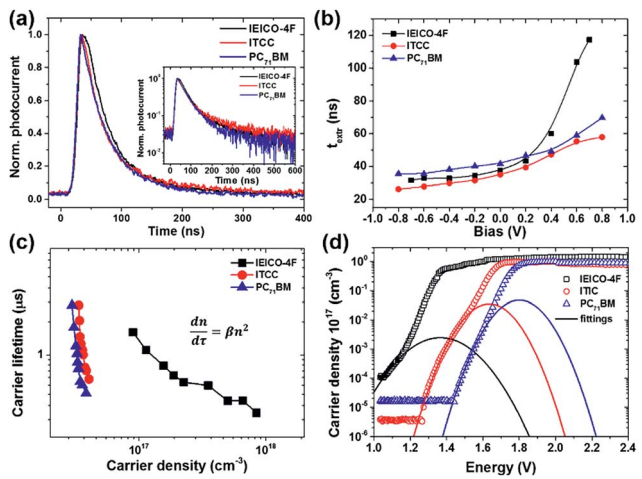

Fig. 5 (a) Normalized photocurrent decay kinetics for various solar cells measured at short-circuit conditions under excitation at 488 nm. Inset: non-normalized photocurrent decay traces in the semi-logarithm scale. (b) Charge extraction time as a function of bias in different solar cells. (c) Recombination kinetics of solar cells with various photoactive layers. (d) Fourier transform photocurrent spectra of solar cells alongside fittings to the Marcus equation.

To allow for a more straightforward assessment of the recombination kinetics, we determined the carrier lifetime (τ_{carr}) and charge carrier density, $n(p)$ in operational solar cells with irradiation (P_{light}) dependent impedance spectroscopy (IS) at open-circuit conditions (Nyquist plots of impedance spectra at different P_{light} are provided in Fig. S5a, ESI†). The carrier density was determined by integrating the chemical capacitance (C_n) over the voltage from dark to V_{oc} based on the relationship described as follows:[34]

$$n(p) = \frac{1}{qAd}\int_{dark}^{V_{oc}} C_n(V)\mathrm{d}V \quad (2)$$

In which A and d are the effective device area and BHJ film thickness, respectively. The τ_{carr} was approximated by the determined C_n and recombination resistance (R_{rec}), according to $\tau_{carr} = R_{rec}C_n$. As seen from the result shown in Fig. S5g (ESI†) the τ_{carr} of all devices exhibits approximately a power law

dependence on the P_{light}. Of interest, the τ_{carr} reduces when the E_g(eff) is reduced. We further determined the carrier density in the solar cells as a function of P_{light} (see results in Fig. S5h, ESI†). With a reduced E_g(eff), the IEICO-4F solar cell possesses the highest $n(p)$ at different P_{light} compared to the other two devices and larger differences in the $n(p)$ are observed at higher P_{light}.

In Fig. 5c, we plotted the determined τ_{carr} against the $n(p)$ at different P_{light}. Based on the general relationship, $dn/d\tau_{carr} = k_{rec}np$, the dependence of k_{rec} on $n(p)$ or the recombination order (RO) can be directly assessed. In all devices, a non-linearity is observed, indicating that the RO is not a constant, but varies with P_{light}. In the compared devices, the RO for all of them is beyond 2, which is suggestive of other recombination channels on top of the bi-molecular recombination. A similar phenomenon has been observed in fullerene devices, which can be ascribed to a couple of reasons, including the effects of trapping and release, morphological traps or spatial inhomogeneity for the distribution of photo-carriers.[31,35,36] Given the insignificant traps indicated by the irradiation dependent V_{oc} (Fig. S5e†), the large RO near 1 sun does not appear to be caused by charge trapping, otherwise severe drops in the FF would occur. To this end, the higher RO could be linked to the spatially non-uniform carrier distribution in our BHJ films.

Lastly, we probed the V_{oc} losses (ΔV_{oc}) in these solar cells. In previous studies, the ΔV_{oc} has been correlated to the energy of the charge transfer states (E_{ct}) formed between neighbouring donor and acceptor molecules,[37] following $\Delta V_{oc} = (1/q)E_{ct} - V_{oc}$.[38] To determine E_{ct}, we performed Fourier transform spectroscopy (FTPS) and the results are shown in Fig. 5d. As can be seen, a wide range of spectral responses was observed with the EQE onset agreeing with the E_g(eff) in the concerned solar cells. The broad shoulder-like features in the low energy regimes can be attributed to the CTS absorption. By means of fittings with the Marcus equation, which is expressed as:

$$\mathrm{EQE} = \frac{f}{E\sqrt{4\pi\lambda k_B T}}\exp\left(\frac{-(E_{CT}+\lambda-E)^2}{4\lambda k_B T}\right) \quad (3)$$

In which E_{ct}, λ, and f are the three fitting parameters, k_B is the Boltzmann constant, and T is the absolute temperature, the E_{ct} can be determined as a fitting parameter from the low energy part of the FTPS measurements (see obtained fitting parameters in Table 2). In our devices, the E_{ct} is larger than the corresponding E_g(eff) and the difference between the two parameters appears to be system-dependent. Based on the determined E_{ct}, we estimated ΔV_{oc} and the results are summarized in Table 2. The ΔV_{oc} of the ITCC and $PC_{71}BM$ solar cells is in line with the empirical relationship $qV_{oc} = E_{ct} - 0.6$, established for a variety of fullerene based devices.[14] Despite the large LUMO–LUMO offset in the UN-BH OSC that constitutes a significant portion of the energy losses, we attained a very low ΔV_{oc} of 0.36 V with respect to the E_{ct} in the IEICO-4F based cell. In a previous study, it has been shown that a rise in the E_{ct} tends to be associated with the reduction of the non-radiative recombination losses of V_{oc} ($\Delta V_{non\text{-}rad}$).[39] To this end, it appears that the portion of $\Delta V_{oc,non\text{-}rad}$ in the total voltage loss may increase when using IEICO-4F. Thus, to further reduce these losses and increase the V_{oc}, efforts may be dedicated to increasing the emission at CTS, described by EQE_{EL}, according to the relationship $\Delta V_{non\text{-}rad} = -(kT/q)\ln(EQE_{EL})$.[40]

In addition to the E_{ct}, the FTPS measurements enabled us to assess the Gaussian width of the density states for the CTS, described by the parameter of λ. The origins of λ have been related to the structural relaxation and energetic disorder at the D/A interface.[41] A smaller λ is generally benign for the delocalization of charge wave functions and the resultant charge dissociations at the D/A interface.[42] The impact of λ becomes more important when the driving force for the exciton dissociation reduces. In our case, the λ (0.296 eV) of IEICO-4F is larger than that with a wider E_g(eff), despite a high J_{sc}. It should be noted that a large LUMO–LUMO offset of 0.55 eV is present in the UN-BG BHJ, with which a geminate recombination is likely insensitive to λ. The higher λ can also be correlated to the morphological features. As shown by the images from the atomic force microscopy (AFM) and the grazing-incidence wide-angle X-ray scattering (GIWAXS) analysis in Fig. S6,† we observed a stronger face-on π–π stacking with a seemingly enhanced molecular ordering in the ITCC-containing BHJ film. This profile, to some degree, agrees with the more efficient charge extraction probed by TPC. While in the PTB7-Th : IEICO-4F blend, a preferential edge-on population appears, which was assigned to lamellar stacking. This somewhat unfavourable morphology may impede the charge extraction at a low electrical field. At this stage, we do not have any evidence for the negative impact of λ on the charge separation in the compared BHJs, at least in geminate processes. In our previous study, we found that the reorganization energy parameter λ can be correlated to the energetic disorder in charge transport.[36] This property is reflected by the Gaussian width of the HOMO (or LUMO) states and can play a role in the ultimate ΔV_{oc}. From this perspective, improving the degree of molecular arrangement in the BHJ film relevant to the charge transport direction may further mitigate voltage losses and increase the efficiency in non-fullerene solar cells.

Table 2 Fitting parameters for FTPS measurements in Fig. 4d with the Marcus equation. Also summarized are the V_{oc} losses (ΔV_{oc}) in the different BHJ solar cells

BHJ	E_{ct} (eV)	λ (eV)	f	ΔV_{oc} (V)
PTB7-Th : IEICO-4F	1.08	0.296	0.00104	0.36
PBDB-T : ITCC	1.645	0.16	0.0195	0.665
PTB7-Th : $PC_{71}BM$	1.48	0.16	0.0131	0.68

Conclusions

To summarize, we have presented an investigation with the aim of understanding the properties of charge transport, extraction, and recombination in UN-BG PTB7-Th : IEICO-4F solar cells that produce an impressive photocurrent with low voltage losses. By comparing the IEICO-4F device to those with mid-gap ITCC and $PC_{71}BM$ acceptors, we found the strongest reduction for the bi-molecular charge recombination in the UN-BG device. This

feature can be correlated to the large J_{sc} corresponding to high incident photon-to-current efficiencies within a wide spectral range. Based on bias-dependent TPC measurements, the IEICO-4F device exhibits an efficient charge sweepout at short-circuit conditions, while this process is impeded by reduced electrical fields. This feature, to some degree, is correlated to a poor FF. From the FTPS measurements, we observed surprisingly low V_{oc} losses of less than 0.4 V in the solar cell with IEICO-4F, compared to the commonly observed ΔV_{oc} amounting to ~0.6 V. We found that with a sufficient energetic offset between the D/A, the reorganization energy λ tends not to be a major limitation for the charge separation. The combination of our analyses highlights several possibilities to further boost the PCE of UN-BG OSCs, for example, by improving the overall charge sweepout efficiency and reducing the bimolecular recombination at low electrical through optimization of the phase segregation and purity in BHJ films. This work enriches our fundamental understanding of the key factors governing photovoltaic behaviours in OSCs based on emerging narrow bandgap electron accepting materials.

Conflicts of interest

There are no conflicts of interest to declare.

Acknowledgements

This work was financially supported by the National Natural Science Foundation of China (No. 21674006, No. 21773045). Y. Z. thanks the 111 Project (B14009). H. Zhou thanks the National Key Research and Development Program of China (2017YFA0206600) and the Chinese Academy of Science (100 Top Young Scientists Program and QYZDB-SSW-SLH033).

Notes and references

1 U. Wurfel, D. Neher, A. Spies and S. Albrecht, *Nat. Commun.*, 2015, **6**, 6951.
2 W. Zhao, S. Li, H. Yao, S. Zhang, Y. Zhang, B. Yang and J. Hou, *J. Am. Chem. Soc.*, 2017, **139**, 7148–7151.
3 Z. Xiao, X. Jia and L. Ding, *Sci. Bull.*, 2017, **62**, 1562–1564.
4 H. Li, Z. Xiao, L. Ding and J. Wang, *Sci. Bull.*, 2018, **63**, 340–342.
5 L. Meng, Y. Zhang, X. Wan, C. Li, X. Zhang, Y. Wang, X. Ke, Z. Xiao, L. Ding, R. Xia, H.-L. Yip, Y. Cao and Y. Chen, *Science*, 2018, **361**, 1094–1098.
6 Z. Xiao, X. Jia, D. Li, S. Wang, X. Geng, F. Liu, J. Chen, S. Yang, T. P. Russell and L. Ding, *Sci. Bull.*, 2017, **62**, 1494–1496.
7 S. Li, L. Ye, W. Zhao, X. Liu, J. Zhu, H. Ade and J. Hou, *Adv. Mater.*, 2017, **29**, 1704051.
8 S. Li, L. Ye, W. Zhao, S. Zhang, S. Mukherjee, H. Ade and J. Hou, *Adv. Mater.*, 2016, **28**, 9423–9429.
9 W. Li, L. Ye, S. Li, H. Yao, H. Ade and J. Hou, *Adv. Mater.*, 2018, **30**, 1707170.
10 J. Sun, X. Ma, Z. Zhang, J. Yu, J. Zhou, X. Yin, L. Yang, R. Geng, R. Zhu, F. Zhang and W. Tang, *Adv. Mater.*, 2018, **30**, 1707150.
11 W. Liu, J. Zhang, Z. Zhou, D. Zhang, Y. Zhang, S. Xu and X. Zhu, *Adv. Mater.*, 2018, **30**, 1800403.
12 X. Li, J. Yao, I. Angunawela, C. Sun, L. Xue, A. Liebman-Pelaez, C. Zhu, C. Yang, Z.-G. Zhang, H. Ade and Y. Li, *Adv. Energy Mater.*, 2018, 1800815.
13 Z. Luo, C. Sun, S. Chen, Z.-G. Zhang, K. Wu, B. Qiu, C. Yang, Y. Li and C. Yang, *Adv. Energy Mater.*, 2018, 1800856.
14 D. Veldman, S. C. J. Meskers and R. A. J. Janssen, *Adv. Funct. Mater.*, 2009, **19**, 1939–1948.
15 W. Li, K. H. Hendriks, A. Furlan, M. M. Wienk and R. A. Janssen, *J. Am. Chem. Soc.*, 2015, **137**, 2231–2234.
16 Y. Li, L. Zhong, B. Gautam, H.-J. Bin, J.-D. Lin, F.-P. Wu, Z. Zhang, Z.-Q. Jiang, Z.-G. Zhang, K. Gundogdu, Y. Li and L.-S. Liao, *Energy Environ. Sci.*, 2017, **10**, 1610–1620.
17 F. Liu, Z. Zhou, C. Zhang, J. Zhang, Q. Hu, T. Vergote, F. Liu, T. P. Russell and X. Zhu, *Adv. Mater.*, 2017, **29**, 1606574.
18 S. Dai, T. Li, W. Wang, Y. Xiao, T. K. Lau, Z. Li, K. Liu, X. Lu and X. Zhan, *Adv. Mater.*, 2018, **30**, 1706571.
19 W. Wang, C. Yan, T. K. Lau, J. Wang, K. Liu, Y. Fan, X. Lu and X. Zhan, *Adv. Mater.*, 2017, **29**, 1701308.
20 Y. Huifeng, C. Yong, Y. Runnan, G. Bowei, Z. Hao and H. Jianhui, *Angew. Chem., Int. Ed.*, 2017, **56**, 3045–3049.
21 X. Song, N. Gasparini, L. Ye, H. Yao, J. Hou, H. Ade and D. Baran, *ACS Energy Lett.*, 2018, **3**, 669–676.
22 S. H. Liao, H. J. Jhuo, Y. S. Cheng and S. A. Chen, *Adv. Mater.*, 2013, **25**, 4766–4771.
23 Z. Zheng, R. Wang, H. Yao, S. Xie, Y. Zhang, J. Hou, H. Zhou and Z. Tang, *Nano Energy*, 2018, **50**, 169–175.
24 W. L. Leong, S. R. Cowan and A. J. Heeger, *Adv. Energy Mater.*, 2011, **1**, 517–522.
25 C. G. Shuttle, R. Hamilton, B. C. O'Regan, J. Nelson and J. R. Durrant, *Proc. Natl. Acad. Sci. U. S. A.*, 2010, **107**, 16448–16452.
26 G. Lakhwani, A. Rao and R. H. Friend, *Annu. Rev. Phys. Chem.*, 2014, **65**, 557–581.
27 S.-H. Liao, H.-J. Jhuo, Y.-S. Cheng and S.-A. Chen, *Adv. Mater.*, 2013, **25**, 4766–4771.
28 H. Yao, L. Ye, J. Hou, B. Jang, G. Han, Y. Cui, G. M. Su, C. Wang, B. Gao, R. Yu, H. Zhang, Y. Yi, H. Y. Woo, H. Ade and J. Hou, *Adv. Mater.*, 2017, **29**, 1700254.
29 V. D. Mihailetchi, L. J. A. Koster, P. W. M. Blom, C. Melzer, B. de Boer, J. K. J. van Duren and R. A. J. Janssen, *Adv. Funct. Mater.*, 2005, **15**, 795.
30 C. Tanase, E. J. Meijer, P. W. M. Blom and D. M. de Leeuw, *Phys. Rev. Lett.*, 2003, **91**, 216601.
31 N. Gasparini, X. Jiao, T. Heumueller, D. Baran, G. J. Matt, S. Fladischer, E. Spiecker, H. Ade, C. J. Brabec and T. Ameri, *Nat. Energy*, 2016, **1**, 16118.
32 P. Zalar, M. Kuik, N. A. Ran, J. A. Love and T.-Q. Nguyen, *Adv. Energy Mater.*, 2014, **4**, 1400438.
33 G.-J. A. H. Wetzelaer, N. J. Van der Kaap, L. J. A. Koster and P. W. M. Blom, *Adv. Energy Mater.*, 2013, **3**, 1130–1134.
34 Y. Zhang, X.-D. Dang, C. Kim and T.-Q. Nguyen, *Adv. Energy Mater.*, 2011, **1**, 610–617.

35 T. Kirchartz and J. Nelson, *Phys. Rev. B: Condens. Matter Mater. Phys.*, 2012, **86**, 165201.
36 A. Baumann, T. J. Savenije, D. H. K. Murthy, M. Heeney, V. Dyakonov and C. Deibel, *Adv. Funct. Mater.*, 2011, **21**, 1687–1692.
37 S. Xie, Y. Xia, Z. Zheng, X. Zhang, J. Yuan, H. Zhou and Y. Zhang, *Adv. Funct. Mater.*, 2018, **28**, 1705659.
38 H. Zhang, S. Li, B. Xu, H. Yao, B. Yang and J. Hou, *J. Mater. Chem. A*, 2016, **4**, 18043–18049.
39 J. Benduhn, K. Tvingstedt, F. Piersimoni, S. Ullbrich, Y. Fan, M. Tropiano, K. A. McGarry, O. Zeika, M. K. Riede and C. J. Douglas, *Nat. Energy*, 2017, **2**, 17053.
40 P. W. Blom, V. D. Mihailetchi, L. J. A. Koster and D. E. Markov, *Adv. Mater.*, 2007, **19**, 1551–1566.
41 K. Vandewal, K. Tvingstedt, A. Gadisa, O. Inganäs and J. V. Manca, *Phys. Rev. B: Condens. Matter Mater. Phys.*, 2010, **81**, 125204.
42 A. C. Jakowetz, M. L. Böhm, J. Zhang, A. Sadhanala, S. Huettner, A. A. Bakulin, A. Rao and R. H. Friend, *J. Am. Chem. Soc.*, 2016, **138**, 11672–11679.